Mater Struct (2024) 57:39
https://doi.org/10.1617/s11527-023-02281-y

ORIGINAL ARTICLE

Water vapour permeability of inorganic construction materials

Christopher Hall · Gloria J. Lo · Andrea Hamilton

Received: 6 June 2023 / Accepted: 29 November 2023

Abstract Water vapour permeability (WVP) data on brick, stone, plaster and cement-based materials from some seventy publications are reviewed and assessed. Almost all sources use standard cup-test methods or close variants. Comparisons of WVP values from different sources on similar materials confirm that reproducibility between different laboratories is poor. Some deficiencies of cup-test methods are discussed, including uncertainties arising from the use of saturated-salt humidistats and desiccants. There is evidence that the water vapour resistance factor decreases as volume-fraction porosity increases, and data support a simple porosity–tortuosity relation. Data also show that the resistance factor decreases with increasing mean relative humidity across the test specimen, with the wet-cup value consistently lower than the dry-cup values for a given material. The contribution of liquid film flow to mass transfer is discussed. It is shown how film thickness and film-flow permeability may be estimated from the water-vapour sorption isotherm; and a related regression equation is developed It is concluded that available data are inadequate to establish the fundamental physics of WVP; vapour-only permeability data for engineering purposes should be obtained in dry-cup tests at low humidity; and research studies should aim to integrate the WVP into the framework of unsaturated flow theory.

Keywords Water vapour permeability · Water vapour diffusivity · Water vapour resistance factor · Cup test · Humidity · Porosity · Film flow · Sorption isotherm · Schirmer equation

Abbreviations

AAC	Autoclaved aerated concrete
CS	Calcium silicate hydrate insulation board
GAB	Guggenheim–Anderson–de Boer
OPC	Ordinary portland cement
WVP	Water vapour permeability

List of symbols

a_s	Specific surface area ($m^2\ kg^{-1}$)
b	Schirmer exponent
c_G	GAB parameter
c_w	Mass concentration of water vapour ($kg\ m^{-3}$)
D_v	Water vapour permeability (s)

C. Hall (✉)
School of Engineering, University of Edinburgh, The King's Buildings, Edinburgh EH9 3FB, UK
e-mail: christopher.hall@ed.ac.uk

G. J. Lo · A. Hamilton
Department of Civil and Environmental Engineering, University of Strathclyde, 75 Montrose Street, Glasgow G1 1XJ, UK
e-mail: glo.lo@strath.ac.uk

A. Hamilton
e-mail: andrea.hamilton@strath.ac.uk

Published online: 26 February 2024

D_{vf}	Film-flow contribution to permeability (s)
D_w	Diffusivity of water vapour ($m^2\ s^{-1}$)
$D_w(0, 1)$	Water vapour diffusivity in still air at temperature 0 °C ($m^2 s^{-1}$)
D_{wf}	Film-flow contribution to diffusivity ($m^2\ s^{-1}$)
f	Volume fraction porosity
F	Mass fraction water content
F_v	Liquid film cross-section area per unit bulk cross-section area
g	Standard acceleration due to gravity ($m\ s^{-2}$)
G	Geometrical tortuosity factor
H	Fractional humidity RH/100
H_c	Lower bound H for capillary condensation
H_m	H at monolayer coverage
$\overline{H}$	Mean of cup H and chamber H
j_m	Mass flux of water ($kg\ m^{-2}\ s^{-1}$)
j_{mf}	Mass flux of water in liquid film ($kg\ m^{-2}\ s^{-1}$)
k_G	GAB parameter
K_f	Film hydraulic conductivity ($m\ s^{-1}$)
Kn	Knudsen number λ/Λ
L	Length (m)
m	Archie law exponent
m_G	GAB parameter
M_w	Molar mass of water ($kg\ mol^{-1}$)
N_A	Avogadro constant (mol^{-1})
p_c	Liquid water capillary pressure (Pa)
p_w	Vapour pressure of water (Pa)
p_{w0}	Saturated vapour pressure of water (Pa)
P	Total pressure (Pa)
q	Parameter of Iversen tortuosity model
$\mathbf{R}$	Gas constant ($J\ mol^{-1}\ K^{-1}$)
r_{wd}	Denotes quantity μ_{wet}/μ_{dry}
RH	Relative humidity (percent)
RH_c	Lower bound RH for capillary condensation
RH_m	RH at monolayer coverage (percent)
$\overline{RH}$	Mean of cup RH and chamber RH (percent)
$\overline{RH}_{wet}$	Wet-cup $\overline{RH}$ (percent)
T	Thermodynamic temperature (K)
x	Space coordinate (m)
α	Denotes quantity $\mathbf{R}T/(M_w g)$ (m)
β	Quantity defined in Eq. 13 (s)
δ	Film thickness (m)
η	Dynamic viscosity of liquid water (Pa s)
λ	Mean free path water in air (m)
Λ	Characteristic length (length scale) of porosity (m)
μ	Water vapour resistance factor
μ_{dry}	Dry-cup resistance factor
μ_{wet}	Wet-cup resistance factor
Ψ	Hydraulic potential (m)
ρ_w	Density of liquid water ($kg\ m^{-3}$)
σ_w	Surface tension of liquid water ($N\ m^{-1}$)
τ	Tortuosity
θ	Volume fraction water content
θ_m	θ at monolayer coverage

1 Introduction

The water vapour permeability (WVP) is a material property used in building physics, in particular in hygrothermal analysis of building performance and in related engineering design models. The WVP describes the rate of transport of water vapour within a porous material under a humidity gradient at constant temperature. The WVP is almost always measured by one of several long-established standard 'cup-test' methods [1–4], all of which are similar to a procedure originally described some sixty years ago [5]. Although used for many decades, the cup test has been shown often [6–9] to be of poor reproducibility between laboratories, although repeatability within a single laboratory may be good. It is surprising that despite this long history of use there has not previously been a review of published WVP data. Our aim here is to gather together the measured WVP values of inorganic materials from a wide range of literature sources and to consider the variation and consistency of these in groups of similar materials. We use the published data to examine how WVP values depend on specimen porosity and on the humidity conditions used. We comment also on the uncertainties in the humidity of saturated salt solutions, a matter not discussed elsewhere, and make several recommendations about the reporting of WVP data.

2 Measurement

2.1 Definitions and theory

In standard cup tests, the gradient of water vapour pressure is created by sealing a specimen of the test material of uniform thickness over the mouth of a cup containing either a saturated salt solution or a desiccant which acts as an internal humidistat to provide a constant relative humidity (RH).The relative humidity $\mathrm{RH} = 100 \cdot p_\mathrm{w}/p_{\mathrm{w}0}$ where p_w is the vapour pressure of water over the saturated salt solution or desiccant, and $p_{\mathrm{w}0}$ is the saturated vapour pressure of pure water both at the same temperature. The cup/specimen assembly is then placed in a closed chamber kept at a different RH, and all maintained at constant temperature. The rate of transfer of water through the specimen is measured by weighing the cup from time to time. If the different RHs of cup and chamber are both constant, there is a constant RH gradient across the specimen, and a steady state is established. The steady rate of change of the weight of the cup provides the primary measurement from which the WVP is calculated. When the RH inside the cup is greater than that in the external chamber, water transfer is outwards and the test is described as wet-cup; in a dry-cup test, the cup contains a desiccant (or less commonly a saturated salt solution of low RH), and the direction of mass transfer is inwards into the cup.

Figure 1a is a schematic of the test arrangement. The underpinning theory is a simple application of Fick's first law by which the mass flux j_m is

$$j_\mathrm{m} = -D_\mathrm{w}\frac{\mathrm{d}c_\mathrm{w}}{\mathrm{d}x}, \tag{1}$$

where c_w is the mass concentration of water vapour and D_w is the diffusivity of water vapour in air (dimension $\mathsf{L}^2\mathsf{T}^{-1}$). To express the flux in terms of the water vapour pressure p_w, we note that c_w is the same as the water vapour density and therefore assuming ideal gas behaviour $c_\mathrm{w} = p_\mathrm{w}M_\mathrm{w}/(\mathbf{R}T)$, where M_w is the molar mass of water, $\mathbf{R}$ the gas constant and T the thermodynamic (kelvin) temperature. Then we have from Eq. 1

$$j_\mathrm{m} = -\frac{D_\mathrm{w}M_\mathrm{w}}{\mathbf{R}T}\cdot\frac{\mathrm{d}p_\mathrm{w}}{\mathrm{d}x} = -D_\mathrm{v}\frac{\mathrm{d}p_w}{\mathrm{d}x} = D_v\frac{p_{\mathrm{wA}} - p_{\mathrm{wB}}}{L}. \tag{2}$$

The composite (lumped) quantity $D_\mathrm{v} = D_\mathrm{w}M/(\mathbf{R}T)$ is the water vapour permeability (dimension T; unit s, but often written as kg (m Pa s)$^{-1}$). In denoting the WVP as D_v we follow common practice [10], but the symbol δ_p is sometimes used, for example in [1, 3].

As noted elsewhere [10–13], the WVP is not a permeability in the Darcian sense of advection in response to a gradient of total hydraulic pressure, but rather it is a tracer diffusivity. In Fig. 1a, the mass flux arises from molecular diffusion of dilute water vapour in air, where the air is essentially stationary. We discuss later whether this simple Fick's law theory provides an adequate description of the cup test. A typical test arrangement is shown in Fig. 1b.

2.2 Water vapour resistance factor

Cup test results are often reported as the water vapour resistance factor $\mu = D_{\mathrm{w}0}/D_\mathrm{w}$, where $D_{\mathrm{w}0}$ is the water vapour diffusivity in still air at the temperature T and atmospheric pressure P at which the cup test was carried out. In building physics, $D_{\mathrm{w}0}$ is usually calculated from an empirical equation proposed in 1938 by Schirmer [14] who reviewed the sparse experimental data then available. This equation is of the form

$$D_{\mathrm{w}0}(T,P) = D_\mathrm{w}(0,1)P'\left(\frac{T}{T_0}\right)^b \tag{3}$$

where $D_\mathrm{w}(0,1)$ is the water vapour diffusivity in still air at temperature $T_0 = 273.15$ K (0°C) and total pressure $P_0 = 1$ atm, and where $P' = P_0/P$. Schirmer recommended the values $D_\mathrm{w}(0,1) = 2.306\times10^{-5}$ m^2 s^{-1}, and $b = 1.81$. In 1998 Massman [15], with the benefit of many new experimental data, supported the use of Eq. 3, retaining Schirmer's b exponent but recommending a lower value of $D_\mathrm{w}(0,1) = 2.178\times10^{-5}$ m^2 s^{-1}. Most recently, Hellmann [16] has calculated the water vapour diffusivity of water in air from molecular kinetic theory. Over the temperature range of interest in building physics (say −40 to +60 °C), Hellmann's results agree closely with those of Massman, and when fitted to Eq. 3 yield $D_\mathrm{w}(0,1) = 2.154\times10^{-5}$ m^2 s^{-1} and $b = 1.91$ (our calculation). In this review we use the Hellmann parameter values, but it is remarkable that the Schirmer equation has proved so accurate. The water vapour permeability $D_{\mathrm{v}0}(T,P)$ derived from the Hellmann values is given by the interpolating equation

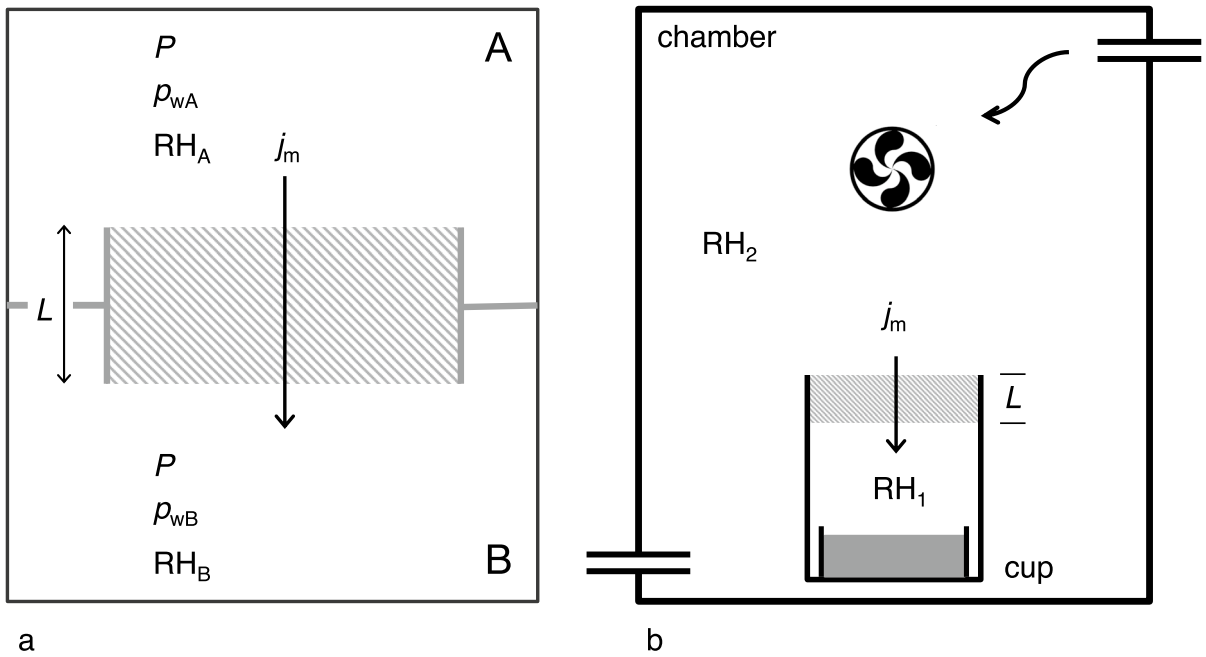

Fig. 1 Water vapour diffusion through a porous material. (**a**) Schematic of water vapour diffusion mass flux j_m in a porous barrier of thickness L separating air-filled compartments A and B with water vapour pressures $p_{wA} > p_{wB}$, relative humidities $RH_A > RH_B$ and total pressure P. (**b**): Typical test arrangement, with dry-cup containing saturated salt solution or desiccant at RH_1 in a chamber with dynamic humidity control at $RH_2 > RH_1$; alternatively, the chamber humidity may be maintained by a second saturated salt solution; not to scale

$$D_{v0}(T,P) = 2.154 \times 10^{-5} \cdot \frac{MP'}{\mathbf{R}T}\left(\frac{T}{T_0}\right)^{1.91} \quad (4)$$

where M is the molar mass of water, 0.018015 kg mol^{-1}, and $\mathbf{R}$ the gas constant 8.3145 J mol^{-1} K^{-1}). The values of D_{w0} and D_{v0} calculated from the reference correlations of Hellmann, Massman and Schirmer are compared in Table 1 for several temperatures.

In ASTM E96 [1] the permeability of still air, there denoted δ_a, is calculated from an interpolating equation equivalent to $\delta_a = D_{w0} \cdot M/(\mathbf{R}T) = D_{v0}$, where D_{w0} is given by Eq. 3, with the Schirmer values of $D_w(0,1)$ and b. The corresponding equation in ISO 12572 [3] contains several errors and cannot be used for calculation, as comparison with the ASTM equation for δ_a or with Eq. 4 shows.

Uncertainty in the value of D_{w0} (or equally in D_{v0}) contributes to uncertainty in the value of the resistance factor μ. Table 1 shows that the Schirmer values of D_{w0} are about 6 percent larger than the preferred values of Hellmann (or of Massman, which for practical purposes in building physics are the same). Hellmann estimates that the expanded ($k = 2$) uncertainty in D_{w0} calculated from Eq. 3 is 3 percent at $T < 300$ K and 2 percent at $T > 300$ K. Using Hellmann (or Massman) values rather than Schirmer values achieves a small but useful improvement in the accuracy of estimates of μ.

2.3 Critique of test methods

Deficiencies of the cup test have often been discussed (notably in [5–7, 11, 12, 17–19]). The most serious of the shortcomings [12] lies in the lack of control of water vapour pressure p_w (or RH) at the specimen surface, especially in the interior of the cup. Since there is a mass flux from the surface of the salt solution or desiccant to the surface of the specimen, there must necessarily be an RH gradient within the cup, and therefore the RH at the surface of the test specimen must be different from that of the humidistat itself. Similar issues may arise on the outer surface of the specimen, depending on how the humidity is

Table 1 Water-vapour diffusivity and water vapour permeability in still air at 1 atm pressure

	$10^5 D_{w0}$ ($m^2\ s^{-1}$)				$10^{10} D_{v0}$ (s)				
	–20 °C	0 °C	20 °C	25 °C		0 °C	20 °C	25 °C	
Hellmann [16]	1.861	2.157	2.470	2.550	1.593	1.711	1.825	1.853	Note 1
Massman [15]	1.898	2.178	2.475	2.552	1.625	1.728	1.829	1.845	
Schirmer [14]	2.009	2.306	2.620	2.702	1.720	1.829	1.937	1.963	Note 2

(1) For the temperature range of interest, at most −40 to +60 °C, Hellmann's interpolating equations for D_{v0} (equations 16 and 17 of [16], valid for a large temperature range), are indistinguishable from the simpler Eq. 4 derived here. (2) These values are the same as can be calculated from Eq. 5 of ASTM E96 [1]

controlled in the chamber. These problems are recognised in at least one standard [3] which describes a time-consuming method using specimens of different thicknesses to correct for the associated error. This correction is rarely mentioned in WVP publications, and it seems unlikely that it is often applied.

Other deficiencies lie in practical issues such as specimen sealing and specimen geometry that have often been noted, for example in [6, 7]. Here we discuss an important aspect of humidity control which has not been considered in earlier publications.

2.4 Humidity control

We note that there are some inconsistencies in the RH values assigned to several of the saturated-salt humidistats used in the cup test. In most cases, the values employed can be traced to the 1977 tabulation of Greenspan [20] (and reproduced in [21]). Since that date, there has been much new work, both experimental and theoretical, on the properties of aqueous electrolyte solutions. We comment on two favoured saturated salt systems.

Potassium nitrate KNO_3. This is a wet-cup humidistat frequently used, and recommended in ISO 12572. Greenspan gives its RH at 20 °C as 94.62 percent and at 25 °C as 93.58 percent (but given as 93.2 percent at 20 °C in EN 1015). Several more recent publications [22–27] have found lower values in the range 91.7–92.7 at 25 °C.

Lithium chloride LiCl This salt is recommended in EN 1015, where the RH of its saturated solution at 20 °C is given as 12.4 percent. The Greenspan RH is 11.31 percent at 20 °C, and 11.28 at 25 °C. The use of LiCl is complicated by the existence of several hydrates, notably the dihydrate $LiCl.2\,H_2O$, stable below 19–20 °C [28, 29], and the monohydrate $LiCl.H_2O$, stable above that temperature. It is likely that in cup tests using lithium chloride the solid phase present in the saturated slurry is the monohydrate, for which a recent estimate of the slurry RH [29] is close to the Greenspan value at 25 °C but a little lower (10.99) at 20 °C. Experimental measurements of vapour pressures over saturated LiCl solutions are somewhat erratic, suggesting the occasional presence of metastable hydrates. Other estimates [23, 30] of the RH of the saturated solution lie in the wider range 11.1–12.1 percent at 25 °C.

Desiccants Other uncertainties are associated with the use of dry-cup desiccants such as silica gel and calcium chloride. Silica gel is not a true phase-invariant humidistat and does not provide a constant RH independent of its water content: the contiguous RH rises continuously as the amount of adsorbed water in the desiccant increases [31]. To maintain an RH below 1 percent at 25 °C, it is necessary to limit the amount of adsorbed water to about 1.3 percent of the weight of the dry silica gel. At 5 percent by weight of adsorbed water the RH has risen to about 5.5 percent, the exact relation depending on the grade of silica gel used [32].

In contrast, calcium chloride $CaCl_2$ can perform as a low-RH humidistat when dry: in the temperature range 15–30 °C, anhydrous $CaCl_2$ takes up water to form a series of hydrates [33, 34]. Provided that at least some of the unhydrated salt is present, the water vapour pressure is stable and the RH < 0.7 percent. However when all the anhydrous solid has been converted to the highest hydrate, $CaCl_2.6\,H_2O$, humidity rises until the deliquescence RH is reached at about 28 percent at 25 °C.

Magnesium perchlorate $Mg(ClO_4)_2$ (listed in ISO 12572 and EN 12086 [35]) behaves similarly [36, 37]. Provided that the desiccant has not absorbed enough water to convert entirely to the hexahydrate

(about 48 percent by weight) it maintains an RH ≤ 0.2 percent at 25 °C.

It is beyond our scope here to determine the preferred values of the RH of saturated salt solution humidistats in the light of current knowledge, but this task now seems overdue. Likewise a more precise statement of the RH established by the commonly used desiccants would be timely.

3 Review of published WVP data

3.1 Scope and general remarks

For this review, we have identified some 70 published reports that contain primary WVP data on inorganic construction materials. (In this task we have benefited from a recent survey [38] of humidity-related properties of plasters). We have also included some data from [39] that are collated from earlier sources, including [40], and some of which are unpublished and otherwise inaccessible. Several commercial databases to which we do not have access, and which in any case contain mostly secondary data, have not been considered. We have not included inorganic-organic composite materials with large amounts of organic component. Thus materials such as hemp-lime plasters are excluded. Organic materials often contain components (notably cellulosics) which take up water in rather different ways from inorganic materials and are subject to swelling. Other organic materials, such as the common synthetic polymers, are strongly hydrophobic, and their surface interactions with water at molecular level are fundamentally different from those of inorganic mineral-based materials.

The quality of the primary reports is variable. Some general observations about these sources of data follow.

- Building conservation provides the motivation and context for the majority of studies. There are numerous reports of the WVP of plasters and building stones, while data on concrete are scanty, and on brick are unexpectedly rare.
- Almost all studies use a standard cup-test method or a variant of it; most commonly this is ISO 12572 [3], in a few cases EN 1015 [2] or ISO 12086 [35]. ASTM E96 [1] is little mentioned. Non-standard experimental procedures are few [13, 41–43].
- Many reports provide either wet-cup or dry-cup data, but few give both; only rarely are tests carried out at more than two sets of RH conditions (but see [8, 44]). In some cases, the RH conditions in the cup and/or chamber are not stated or not specified adequately.
- Across all materials, wet-cup measurements are twice as numerous as dry-cup.
- Often the composition of the test materials is poorly characterised in respect of mineralogy and/or mix composition (notable exceptions are [45–48]). When this information is absent, it is impossible to develop any physicochemical understanding of WVP behaviour.
- In nearly all cases the atmospheric pressure correction [3, 13] is not mentioned, although it may or may not have been applied; often the test temperature is not stated, although it may be implied by reference to a standard test method.
- In a few cases, there are internal inconsistencies in the data, and these datasets have been excluded.
- Often, there are no estimates of uncertainty or error.
- Many reports provide porosity data; where porosities are not given (or cannot be estimated from density data) our analysis of the WVP data has been limited. A few publications provide sorption isotherm data (see for example [42, 49]). Data on specific surface area are rare.
- Statistical analyses of WVP data in relation to other thermophysical properties are infrequent, but see [50, 51].
- There is often no comparison of results with prior published data on similar materials (but for example see [47]).
- There are few theoretical discussions or analyses, a feature which highlights the lack of an accepted physically based model of vapour diffusion/permeability in construction materials. Exceptions are [44, 52–54]. There are only infrequent references to publications on diffusion in porous media from outside the field of construction materials.
- Of the sources identified, only about one third provide adequate data for analysis. These yield a dataset of about 350 individual WVP measurements on a wide variety of materials.

3.2 Preliminaries

Publications may report one or more of the quantities D_w, D_v and μ. We have chosen mainly to compare the resistance factor μ, since it is a dimensionless number usually in the range 1–50, and is less sensitive to temperature and atmospheric pressure than D_w and D_v. Where sources give only values of μ, we have used those values. Where D_w and/or D_v are given, we have calculated μ using the Hellmann value of D_{w0} and/or D_{v0} at the test temperature (if stated).

The symbol $\overline{\text{RH}}$ is used to designate the mean of the reported values of cup RH and chamber RH. We then classify all datasets where $\overline{\text{RH}} \geq 70$ percent as wet-cup; and all datasets where $\overline{\text{RH}} \leq 45$ percent as dry-cup. The few cases (for example [13, 44, 55]) where data are obtained under conditions where $45 < \overline{\text{RH}} < 70$ percent are unclassified. These definitions of wet-cup and dry-cup conditions are consistent with the usage in standards [1–4, 35]. The terminology is not entirely logical since test results should be independent of the direction of flow (in or out of the cup). The main consideration is the moisture state [10] of the specimen, for which we use $\overline{\text{RH}}$ as a simple metric. In figures, dry-cup data points are plotted as unfilled (open) symbols, and wet-cup as filled symbols.

3.2.1 The role of porosity

In what follows we use the volume-fraction (open) porosity f as one explanatory variable. The open porosity is straightforward to measure, and generally has low uncertainty/error [10, 56, 57]. Within a group of similar materials the rate of water vapour diffusion must tend to increase with the porosity f. In an isotropic material, the available fractional area for transport in any cross-section equals f. Of course, in a random pore structure as f decreases, the meandering path-length penalty or tortuosity τ tends to increase. Therefore on an elementary view of molecular gas diffusion in a porous material [52, 58–62] the diffusivity $D_w \sim f/\tau$ (where $\sim$ denotes varies as or scales as). The tortuosity itself also varies roughly as $1/f^{m-1}$ where m is the Archie law exponent which has a value around 2 [10, 63, 64]. So the elementary model has

$$\mu = D_{w0}/D_w = 1/f^m, \tag{5}$$

for $0 \leq f < 1$ and where $\mu \to 1$ as $f \to 1$ as it must for pure vapour diffusion. Alternatively expressed, $D_w = D_{w0} f^m$, and likewise $D_v = D_{v0} f^m$. Recent analyses [65, 66] broadly support these relations for vapour diffusion. For simple vapour diffusion through a porous material, Eq. 5 is a universal relation with only the single parameter m.

We note three limitations of this model. First, it assumes that molecular-kinetic diffusion is unaffected by the dimensions of the pore structure, specifically that the mean free path of water molecules in air, λ, is smaller than the length scale of the porosity Λ: that is, that the Knudsen number $\text{Kn} = \lambda/\Lambda \ll 1$ [67]. For most of the materials of interest here this is true, although we may expect to find evidence of the transition to Knudsen diffusion in some nanoporous cement-based materials [68], since at 25 °C $\lambda = 0.13$ μm. In such cases the diffusivity is reduced by a factor $1/(1 + \text{Kn})$. Second, the elementary model takes no account of the connectivity of the pore system: for example there are a few high-porosity materials such as aerated concrete in which pores may nevertheless be poorly connected.

3.2.2 The role of humidity

The third limitation of a simple porosity-controlled view of WVP properties, and the one of the most general importance, is that the transport of water through the barrier is assumed to be entirely due to molecular diffusion in the gas/vapour phase. It is often said that there may be a contribution to the transport from capillary flow of liquid water. This is sometimes stated to arise from capillary condensation at higher humidities. In fact, classical pore-filling capillary condensation (in the sense of the Kelvin equation) can be ruled out in materials such as brick, stone, concrete and plasters except at the very highest humidities, say above about 98 percent RH [10] (but with an exception for some cement-based materials [68] where nanopores are filled at lower RH). What cannot be ruled out across a wide range of higher humidities in most materials is the formation of multilayer liquid films by water vapour adsorption [69]. These may indeed contribute to

water transport, thus adding a second term to the denominator of Eq. 5:

$$\mu = D_{w0}/[D_w + D_{wf}(H)] \tag{6}$$

where D_{wf} accounts for the contribution to the diffusivity from film flow. The film diffusivity D_{wf}, dimension $\mathsf{L}^2\mathsf{T}^{-1}$, depends on the fractional humidity $H = \mathrm{RH}/100$ and hence on θ, the volume-fraction water content of the specimen. While D_{w0}/D_w is necessarily ≥ 1, μ as defined in Eq. 6 can now take values < 1 at high humidities.

Equation 6 can equally well be written as

$$\mu = D_{v0}/[D_v + D_{vf}(H)] \tag{7}$$

where the film permeability D_{vf} (dimension T) accounts for the contribution to the WVP from mass transfer in the film. The lower limit to the range of RH in which film flow contributes to the total mass flux is set approximately by RH_m, the RH at which a molecular monolayer of water is formed. The value of RH_m (or $H_m = \mathrm{RH}_m/100$) can be obtained from analysis of the water vapour sorption isotherm, and is usually in the range 15–30 percent RH. The upper limit is set by the RH at which capillary condensation occurs, approximately $\mathrm{RH}_c = 100H_c$ where $H_c = \exp[-2\sigma_w M_w/(\Lambda \mathbf{R} T \rho_w)] = \exp[-1.049 \times 10^{-9}\ \mathrm{m}/\Lambda]$ for water at 25 °C. Here Λ, as previously, is a characteristic length of the pore structure of the material, and ρ_w is the density of liquid water. Broadly speaking we can expect film flow to contribute significantly to the WVP in some or most of the RH range above, say, 60 percent for the inorganic materials of interest here: brick, stone, concrete and plasters.

Several regression or interpolation equations have been used to described the RH dependence of the WVP, for example $\mu = A_1 + B_1 \exp(C_1 \cdot \mathrm{RH})$ in [70], and the reciprocal form

$$\mu = 1/[A_2 + B_2 \exp(C_2 H)] \tag{8}$$

in [39, 40, 53]. These are both empirical equations without clear theoretical basis. The quantities A_1, B_1, C_1 and A_2, B_2, C_2, are regression parameters.

However, it is possible to obtain a physically-based regression equation for the dependence of the WVP resistance factor μ on the relative humidity RH using the theory of flow in liquid films. In recent work on unsaturated flow in soils physically based theoretical relations between film conductivity and film thickness, hydraulic potential and pore size have been developed [71–73]. In these analyses the film thickness is calculated from hydraulic potential. Here we prefer to obtain the film thickness $\delta(H)$ directly from the sorption isotherm $F(H)$ of the material. The basis for this approach is described in Appendix 1, where we show that the quantity D_{vf} in Eq. 7 depends on the fractional humidity H through the isotherm $F(H)$ by the relation $D_{vf} = \beta \cdot F^3/H$. Therefore

$$\mu(H) = \frac{D_{v0}}{[D_v + \beta F^3/H]}, \tag{9}$$

where the quantity β, which does not depend on H, is defined in Appendix 1. For the purposes of obtaining a physically-based regression equation for $\mu(H)$ we use the Guggenheim–Anderson–de Boer [GAB] isotherm model, an approximate form of which can be written $F = m_G/(1 - k_G H)$ (Appendix 1). Then we have from Eq. 9

$$\mu(H) = \frac{1}{[A_3 + (B_3/H)(1 - C_3 H)^{-3}]}, \tag{10}$$

where A_3, B_3 and C_3 are regression parameters. If the GAB parameter k_G is known then $C_3 = k_G$. We test the use of this regression equation below in a small number of cases where WVP data are available.

We next discuss available WVP data on groups of materials.

3.3 Clay brick

WVP data on brick are sparse. Of 11 sources, two are excluded for lack of information on RH test conditions. Notable among the nine retained is a set of wet-cup measurements on thirteen brick ceramics of varied clay composition [50]; and also the round-robin measurements on a single brick material by several laboratories [8, 18, 74]. The WVP data in [39] are collated from four earlier unpublished studies. Figure 2 shows μ versus $1/f$. The range of porosity f, 0.20–0.50, spans that of most commercial bricks [56]. Data are extremely scattered, and there is little or no separation between dry-cup and wet-cup values. There is no clear correlation between μ and $1/f$.

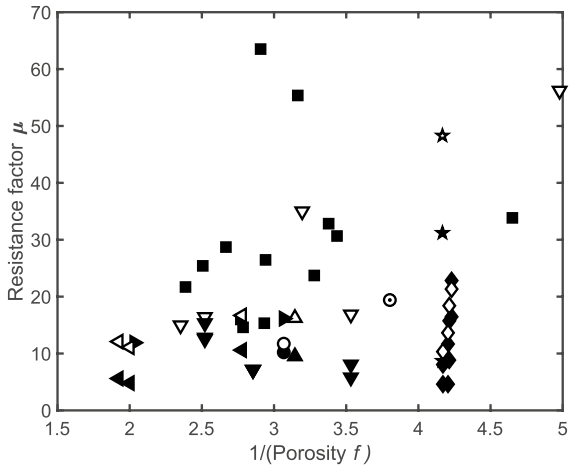

Fig. 2 Water vapour resistance factor μ for fired-clay brick: published data. Key: ■ [50] (assumed to be wet-cup), △ ▲ [75], ☆ ★ [41], ⊙ [74], ○ ● [18], ▶ [51], ◁ ◀ [76], ◆ ◇ [8], ▽ ▼ [39]. For data of [39], porosity f estimated from reported bulk density. Open symbols: dry cup; filled symbols: wet cup. Porosity f decreases from left to right

3.4 Sandstones

There are WVP data on sandstones from 11 sources, one without essential test information. Materials come from several different countries. Figure 3 shows μ versus $1/f$. Here the trends are somewhat clearer than for brick. Dry-cup values of μ lie mostly well above wet-cup values at similar porosity f. In the dataset as a whole wet-cup μ values tend to increase as $1/f$ increases (or as f decreases), although the scatter is too large for a quantitative regression. This trend is also clear in several individual datasets, in particular in the wet-cup data from [44–46]. The trend is also seen in the dry-cup data from [78].

The data spread is considerable, covering the range 0.04–0.31 in f, and 5–155 in μ. Sandstones may be considered as grain packs with well connected porosity [82]. The sandstones of the dataset are varied both mineralogically and microstructurally. Some are quarry materials, while others are recovered from historic buildings. The WVP sandstone data are mostly accompanied by comprehensive characterisation of mineralogy or thermophysical properties, or both.

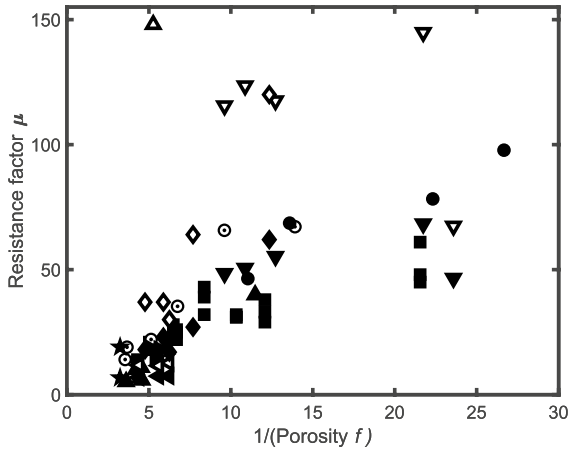

Fig. 3 Water vapour resistance factor μ of sandstones from several countries: published data. Key: German, ■ [45], ▲ [46], ▶ [77]; Czech, ⊙ [78], ◁ ◀ [79], ☆ ★ [80], ▽ ▼ [49]; Chinese, ● [44]; Scottish, ◇ ◆ [47]; French, △ [81]. Open symbols: dry cup; filled symbols: wet cup

3.5 Limestones

Unlike sandstones, limestones have been little studied. Only five sources [51, 77, 81, 83, 84] provide both WVP and porosity data on a total of 14 materials (Fig. 4), reduced further by some duplication between [83] and [84]. All but one are wet-cup μ values. Although meagre, the data may suggest a trend towards higher wet-cup μ as f decreases.

3.6 Lime mortars and plasters

Mortars and plasters made from hydraulic and non-hydraulic (air) limes form the largest subset of WVP data.

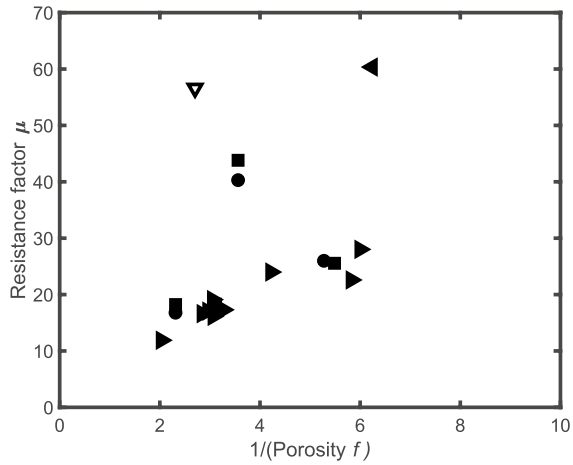

Fig. 4 Water vapour resistance factor μ of limestones: published data. Key: ■ [84], ◀ [77], ▶ [51], ▽ [81], ◆ [85], ● [83] (an extreme outlier at $\mu = 225$, $1/f = 190$ is not shown). Open symbols: dry cup; filled symbols: wet cup

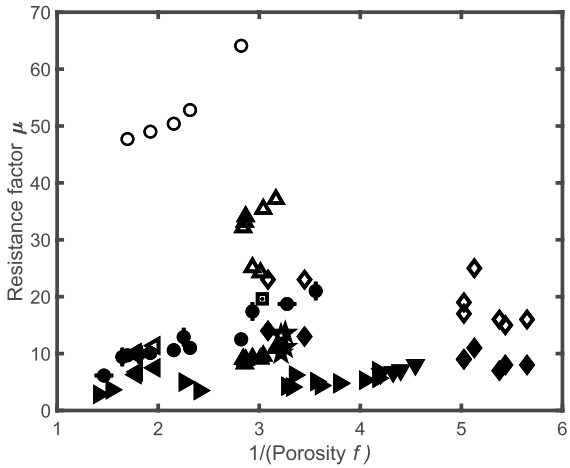

Fig. 5 Water vapour resistance factor μ of lime plasters and mortars: published data. Key: ⊡ [86], ○● [87], △▲ [88], ◇◆ [47], ▶ [89], ▼ [90], –● [51], ⬮ [91], ☆★ [92], ◀◁ [93]. Open symbols: dry cup; filled symbols: wet cup

There are 16 sources. Six of these give incomplete information on test conditions or have errors of calculation. Of those retained, ten provide porosity data, and of these five provide both wet-cup and dry-cup μ values. Figure 5 shows μ versus $1/f$ for these materials. WVP data from an excellent study of repair mortars [48] is not included since the porosity was not measured. The separation of wet-cup and dry-cup values of μ is clear. The wet-cup values are uniformly rather low, with $\mu < 14$ in most materials. There is no trend in the dry-cup μ to higher values as porosity f decreases.

3.7 Cement-based materials

Of twelve reports of WVP in cement-based concretes and mortars, five provide porosity data and complete test details [8, 13, 55, 75, 94, 95], and these are shown in Fig. 6. Only three sources provide dry-cup values. The materials, mixes and compositions are unconventional and the data provide little guidance on the WVP properties of standard cement mortars and concretes. These data support the notion that the resistance factor μ increases as porosity f decreases, but with the caveat that there is no such trend within the individual low porosity and high porosity clusters considered separately. These cement-based materials have the largest range of wet-cup μ values of any of the groups of materials reviewed.

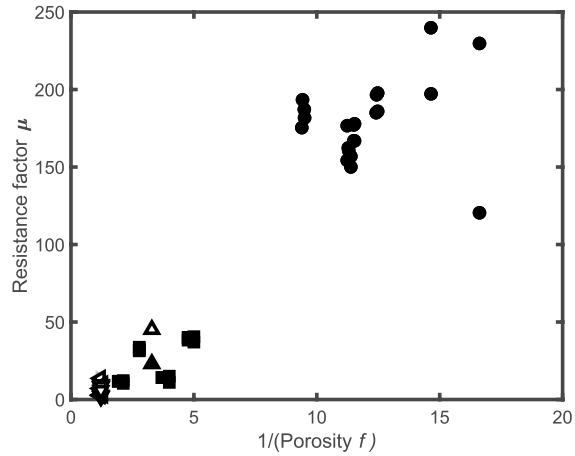

Fig. 6 Water vapour resistance factor μ of cement mortars and concretes: published data. Key: ■ [95] (lightweight mortars, cement:aggregate 3.5:1 by volume), ● [55] (OPC, pozzolan, slag and limestone powder concretes), △▲ [75] (commercial masonry mortar), ▽▼ [8] (AAC), ◁◀ [94] (AAC), ▶ [13] (AAC, RH 54 percent, unclassified). Open symbols: dry cup; filled symbols: wet cup

3.8 Unfired clay materials

WVP data on unfired clays and earth bricks are needed for moisture buffering calculations and there are eight reports of test results on purely inorganic clay materials. Of these three use both wet-cup and

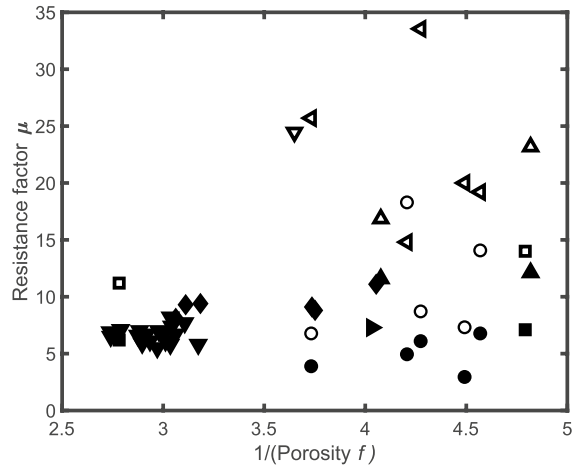

Fig. 7 Water vapour resistance factor μ of unfired clay materials: published data. Key: □■ [96], ○● [97], ◁ [98] (mean μ parallel and normal to extrusion axis), ◆ [99], ▽ [86], △▲ [100], ▼ [101], ▶ [102]. Open symbols: dry cup; filled symbols: wet cup

dry-cup conditions. Three provide porosity data, but others report the bulk density from which a reasonable estimate of the porosity can be made [10], given that kaolinite and quartz are the predominant mineral constituents. Figure 7 shows μ versus $1/f$ for these unfired clay materials. Wet-cup μ values are generally lower than dry-cup values and show little variation with porosity.

3.9 Calcium silicate sheet

Calcium silicate sheet (CS) is a commercial material with an exceptionally high porosity (f 0.89–0.91), formed by hydrothermal reaction and consisting mainly of the fibrous calcium silicate hydrate mineral xonotlite [103, 104]. Four of the six available datasets [8, 13, 18, 74] report measurements on the same CS product, while one other [105] uses closely similar materials. The data (26 values, some no doubt the mean of replicates) include both wet-cup and dry-cup measurements made at several different RH conditions. (Other data [11] on an unspecified calcium silicate insulation material of lower bulk density are included only in Fig. 11). Figure 8 shows the spread of reported μ values plotted against the mean fractional humidity $\overline{H}$. As expected for a material of such high porosity μ is in all cases rather low, but the scatter is considerable. There is a weak trend towards higher μ at lower RH. For this material the ratio $\overline{\mu}_{\mathrm{dry}}/\overline{\mu}_{\mathrm{wet}}$ is about 1.4. We note two wet-cup values of $\mu < 1$ at RH $\approx$ 90 percent. Figure 8 shows a data fit to Eq. 9.

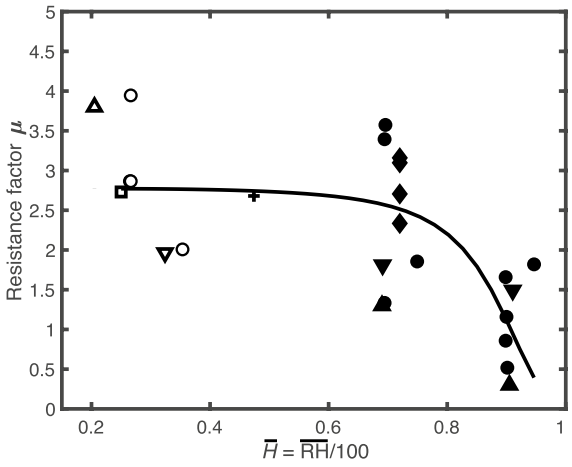

Fig. 8 Water vapour resistance factor μ of calcium silicate sheet: unfilled symbols, dry cup; filled symbols, wet cup; + unclassified; temperature 23 °C except as noted. Key: + [13], 25 °C; ○ ● [8]; □ [106], 25 °C, interpolated; ▽▼ [18]; △ ▲ [74] and Jianhua Zhao, private communication; ◆ [105]. Solid line is a least-squares fit of Eq. 10 to the data, A_3 0.353, B_3 8.19×10^{-4}, $C_3 = k_G$ 0.979 (from authors' unpublished sorption isotherm data)

4 Analysis and discussion

4.1 Dependence of WVP on porosity

Elementary physics requires that pure vapour diffusion in a porous material depends on the volume-fraction porosity f, as indicated in Eq. 5. The data of Figs. 2, 3, 4, 5, 6 and 7 provide some indications of a correlation between WVP and porosity in groups of similar materials, but with much scatter. The trend is clearest in data for sandstones (Fig. 3) and cement-based materials (Fig. 6).

However by taking all the available data together we find stronger evidence of a systematic overall trend of increasing resistance factor μ with decreasing porosity. Fig. 9a, b show composite plots of all WVP data from Figs. 2, 3, 4, 5, 6 and 7 on logarithmic axes. Data from dry-cup and wet-cup tests are plotted separately, with more than twice as many wet-cup data points as dry-cup. While there is some scatter, the trend line for both dry-cup and wet-cup datasets is clear and in broad agreement with Eq. 5, with Archie exponent $m \approx 2$.

Several factors no doubt contribute to the scatter, including those responsible for the poor reproducibility in round-robin tests. The wet-cup values of μ may be reduced by contributions to transport from film-flow, the magnitude of which may vary from material to material. In addition μ may depend on other microstructural and compositional features besides the porosity. A multi-factor analysis [51] of a small suite of limestones, fired-clay bricks, and cement and lime plasters finds that features of the pore-size distribution explain the wet-cup WVP better than porosity alone. A study of fired-clay bricks also shows that WVP values are influenced by the pore-size distribution [50]. Both analyses are based on wet-cup data only, where both vapour and film transport probably occur. We are unable to extend and confirm these analyses here since none of the published sources we review provide pore size data.

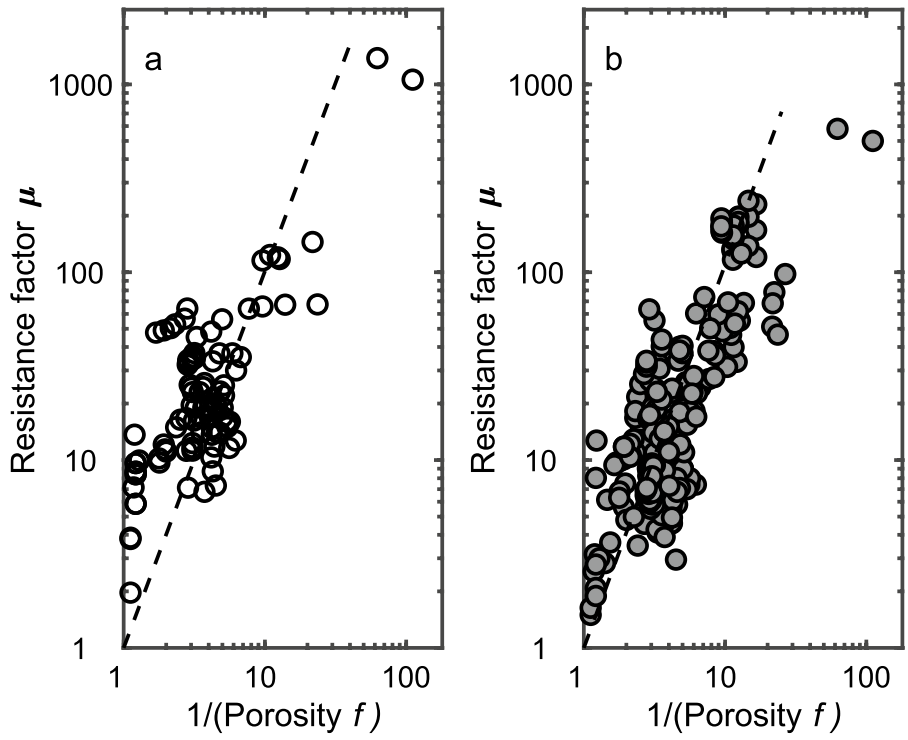

Fig. 9 Water vapour resistance factor μ versus $1/f$: all data from Figs. 2, 3, 4, 5, 6 and 7. Porosity f decreases from left to right. (**a**) Dry-cup (low humidity) data (number of data points $n = 97$); dashed line (- -), Eq. 5 with best fit on log-transformed data $m = 2.01 \pm 0.15$. (**b**) Wet-cup (high humidity) data ($n = 249$); dashed line (- -), Eq. 5 with best fit $m = 1.80 \pm 0.06$

To test Eq. 5 further requires WVP data obtained at low RH where film flow does not occur, ideally on a suite of materials of different porosities but of similar microstructure and tested in the same laboratory. If we consider dry-cup data only, available datasets in which porosity varies between specimens of similar morphology and microstructure are rare [47, 78]. These two datasets, both sandstones, are shown in Fig. 10. The data fit to Eq. 5 is far from conclusive, but provides some support. In this matter also further study is needed.

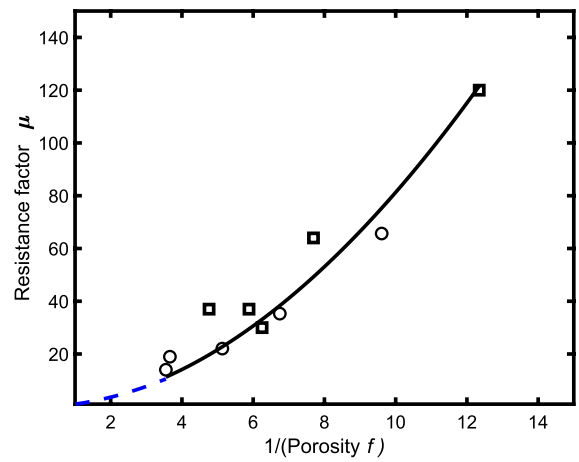

Fig. 10 Variation of dry-cup resistance factor μ of sandstones with porosity f. □ [47]; ○ [78] (one outlier datapoint omitted). Solid line (—): fit to Eq. 5, $m = 1.91$; dotted line (- - -): extension of fitted line to $\mu = 1$ at $f = 1$

4.2 Dependence of WVP on humidity

There is a large subset of reports where both wet-cup and dry-cup WVP data are given (and a few cases where wet-cup data are provided at more than one $\overline{\text{RH}}$). For this subset we calculate the ratio $r_{\text{wd}} = \mu_{\text{wet}}/\mu_{\text{dry}}$. Figure 11 shows r_{wd} versus $\overline{\text{RH}}_{\text{wet}}$. There is no clear clustering of different groups of materials but for the entire dataset $r_{\text{wd}} \leq 1$. That is to say, μ_{wet} is almost always less than μ_{dry}, and usually much less. Taken overall, r_{wd} values are distributed about a mean of 0.58 (s.d 0.21), with range 0.13–1.00. We can say cautiously that the resistance factor at $\overline{\text{RH}} > 70$ percent is often about one-half that at $\overline{\text{RH}} < 45$ percent, but with much scatter in the values reported for individual materials. In this large dataset ($n = 124$) as a whole there is no clear indication of a strong decrease of r_{wd}

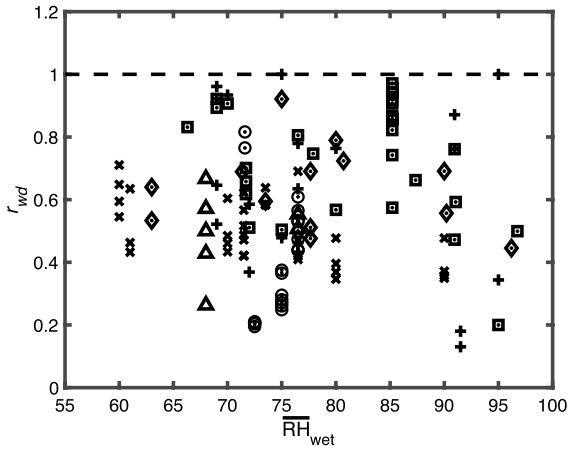

Fig. 11 Ratio $r_{wd} = \mu_{wet}/\mu_{dry}$ of different groups of materials versus $\overline{RH}_{wet}$, the wet-cup mean RH. Symbols: Brick, + [18, 41, 75, 76]; sandstones, × [44, 47, 49, 79, 80]; cement-based materials ⊡ [11, 18, 39, 55, 75, 93]; gypsum, ◇ [39, 107–109]; lime plasters ⊙ [47, 87, 88, 92]; earth bricks △ [96, 97]

with increasing $\overline{RH}_{wet}$ at $\overline{RH} > 55$ percent, although there may be a weak trend to lower r_{wd}. This is contrary to what is sometimes asserted, for example in [39, 110].

Stronger evidence of a rapid decrease in the resistance factor μ at high RH can however be found in the few cases where WVP data have been obtained by an individual laboratory at several RH values on a single material. Notable examples are reported in [11, 39, 40], from which two datasets, one for a concrete and one for calcium silicate CS board, are shown in Fig 12. In Fig 12a we show that the regression equation Eq. 10 describes reasonably well the variation of μ with H at higher humidities. Accordingly, these few data suggest that film transfer makes an increasingly important contribution at RH > 50–60 percent. The last two decades have produced no new data to test this conclusion.

The value of using WVP data from a single source is evident in comparing Fig. 12a with Fig. 8, where the trend of decreasing μ with increasing RH is largely if not entirely masked by the data scatter between laboratories. In Fig. 11 the scatter almost completely conceals any such trend.

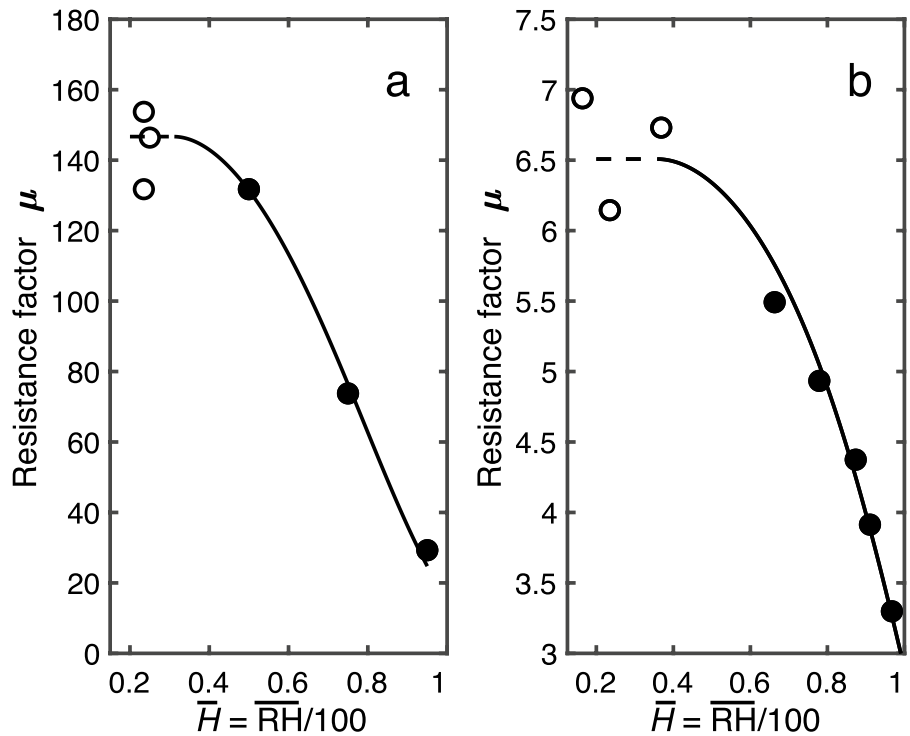

Fig. 12 Variation of resistance factor μ with fractional humidity $\overline{H} = \overline{RH}/100$. Open symbols: dry cup; filled symbols: wet cup. (**a**) Dense concrete [39, 40], ρ_b 2176 kg/m^3: Solid line, fit to Eq. 9, $A_3 = 3.40 \times 10^{-3}$, $B_3 = 4.47 \times 10^{-4}$, $C_3 = 0.807$. (**b**) Calcium silicate sheet [11]: Solid line, fit to Eq. 9, $A_3 = 0.111$, $B_3 = 6.38 \times 10^{-3}$, $C_3 = 0.699$

4.3 Humidity, moisture state and film flow

Figs. 8 and 11 show that WVP data are reported over a wide range of $\overline{\text{RH}}$, from 17 to 98 percent (and cup RH from 0 to 100 percent). This means that the moisture state of the specimen varies widely from test to test. This range of RH is more or less the same as the range spanned in water vapour sorption isotherm measurements on inorganic materials, and from which the variation of equilibrium moisture content is found as a function of RH. From such measurements we know that in brick, stone, concrete and plaster materials, a complete water monolayer is formed at some well defined RH, here denoted RH_m, different for each material but commonly around 15–30 percent, and that as the RH rises beyond RH_m multilayer films of increasing thickness are formed. These may be 5–50 molecular layers thick at the higher RHs (say 80–90 percent), and are liquid films with properties close to those of bulk water. For illustration, the sorption isotherm of the material of calcium silicate sheet has $\text{RH}_\text{m} = 24.0$ percent, at which RH its volume-fraction water content $\theta_\text{m} = 1.4 \times 10^{-3}$ (authors' unpublished data). At 90 percent RH, $\theta_{90} \approx 8.5\,\theta_\text{m}$, the additional adsorbed water forming multilayer films.

Film flow has received little mention in the field of construction materials (but see [111]). In soils, film flow of water is considered to make an important, sometimes dominant, contribution to mass transfer in the range of hydraulic potential $\Psi = 100\text{–}1.5 \times 10^4$ m [69, 71–73], corresponding to RH 99–30 percent. It cannot be assumed that these numbers transfer directly to brick, stone and concrete materials, but they are indicative. We note also that the film conductivity K_f (and hence D_vf) varies not only with Ψ but also with the specific surface area, scaling roughly as Λ^{-1} [71]. The contribution of film flow to mass transfer is therefore greater in fine-pored materials than in coarse-pored because the film area is greater. Film flow depends strongly on pore size as it increases with surface area. In contrast, pure vapour diffusion is generally independent of pore size except in the nanoporosity Knudsen regime.

The film conductivity K_f is also understood to scale as δ^2, where δ is the film thickness, approximately 0.3 nm for each molecular layer [72]. These results suggest that the interpretation of how WVP data vary with RH and and with material composition could usefully draw on information from the sorption isotherm, since this provides information on film thickness and surface area as a function of RH (or H). Parts of that task are implemented in [111] to obtain the film conductivity of several brick and cement-based materials, using however the van Genuchten water retention function $\theta(p_\text{c})$ rather than the sorption isotherm $\theta(H)$.

It is probably only at $\text{RH} < \text{RH}_\text{m}$ that mass transfer occurs entirely by vapour diffusion, so that if a true WVP is required from a cup test it should be obtained by using a humidistats or desiccants that ensure that $\text{RH} < \text{RH}_\text{m}$ on both faces of the specimen. It may be that the chamber RH set-point of 50 percent, widely used in dry-cup tests, is too high.

More generally, it should be recognised that the WVP measured with any particular set of RH test conditions is sampling a value on a continuous hydraulic conductivity function that runs from saturation to dryness.

It is useful to note that the cup-test, for all its drawbacks, has the virtue of establishing a one-dimensional steady-state flow. As such it has a simple solution in unsaturated flow theory [10]. This should allow the conductivity function itself to be obtained from a series of cup-test values of WVP on a material in different moisture states (or $\overline{\text{RH}}$). Much of this was set out in [41], and partially developed in [68, 111, 112].

5 Conclusions

- The review of WVP data published over four decades shows that much of the available information is of poor quality, with many reports lacking information on test conditions and materials.

  There is a large amount of scatter in data on subsets of data on similar materials. This finding is consistent with the poor reproducibility seen in round-robin exercises.
- Despite the scatter, there is evidence of a decrease in resistance factor μ with increasing porosity, as expected from physical arguments. The data tentatively support the use of Eq. 5 to estimate dry-cup WVP properties. If that is confirmed by further study using more accurate WVP data, then good estimates of μ may be obtained from porosity measurements by calculation.

- Similarly the available data as a whole confirm that the wet-cup μ values are consistently lower by a factor of about two than dry-cup values on the same material. Limited data support the notion that transport by flow of adsorbed water films contributes to the total mass flux at higher humidities. We propose here that film thickness and film-flow conductivity can be estimated directly from the water-vapour sorption isotherm of the material. The decrease in μ at high humidity (say RH > 60–70 percent) is sufficiently great that the RH dependence of μ should be allowed for in hygrothermal calculations, and more carefully investigated in WVP cup tests.
- The scatter in WVP data published over many years is unsatisfactory for practitioners and researchers alike. Many of the available WVP data have limited value either for engineering calculation or for research purposes. It is recommended that to obtain engineering data WVP should be measured at low RH where mass transfer occurs by vapour diffusion only. Wet-cup tests should take account of the strong dependence of WVP on RH. It is further recommended that for research purposes the steady-state cup-test configuration should be supported by a comprehensive unsaturated flow theory and experiments should acquire data over a wide range of well-defined moisture states.
- To obtain more reliable data requires improvements in several aspects of the WVP measurement process: the design of test procedures and their practical implementation, the validation and reporting of results, and the reviewing of data before publication. The task of developing and using WVP test methods is hampered by the lack of standard reference materials having well validated and traceable WVP values [113]. We suggest that sintered borosilicate glass filter plates [114] may be suitable for this purpose. These are manufactured in a wide range of pore sizes and with specified air permeabilities.

Acknowledgements We thank J-E Aubert, P Banfill, M Bomberg, M Dondi, Z Pavlik and J Zhao for providing information, and W D Hoff for comments.

Declarations

Conflict of interest The authors have no conflicts of interest to declare that are relevant to the content of this article.

Appendix 1: Isotherms, film thickness and film flow

The film thickness δ and its variation with fractional humidity H can be obtained from the water vapour sorption isotherm $F(H)$, where F is the mass fraction water content at H. To show this, we use the Guggenheim–Anderson–de Boer (GAB) isotherm model. The GAB model, a simple extension of the widely used BET isotherm model, generally represents well the experimental $F(H)$ behaviour of inorganic construction materials up to high RH [10]. The GAB equation is

$$F = \frac{m_G c_G k_G H}{(1 - k_G H)[1 + k_G H(c_G - 1)]}, \tag{11}$$

where m_G, c_G and k_G are dimensionless parameters. The quantity m_G is the mass fraction water content at which a complete monolayer exists. The corresponding fractional humidity at monolayer coverage is $H_m = 1/[k_G(1 + c_G^{1/2})]$, which for inorganic construction materials lies typically in the range 0.15–0.30. The thickness of the monolayer water film is taken as $\delta_m = 0.27$ nm [115] from molecular dimensions. At higher humidities $H > H_m$, the thickness of the water film $\delta = \delta_m F(H)/m_G$. If the specific surface area a_s is known, then $\delta(H) = F(H)/(a_s \rho_w)$. For illustration, Fig. 13 shows how δ varies with H for calcium silicate sheet and a dense concrete, the materials for which WVP data are shown in Fig. 12. For CS, $H_m = 0.24$ and for C, $H_m = 0.30$. For the purpose of calculating the film thickness, the simpler formula $F(H) = m_G/(1 - k_G H)$ is an excellent approximation.

When the film thickness δ is known, standard results from the theory of free-surface liquid film flow (for example [116]) can be used to estimate the liquid permeability of the film

$$k_{mf} = -j_{mf} \frac{dp_c}{dx} = \frac{\rho_w \delta^2}{3\eta}, \tag{12}$$

where p_c is the capillary pressure, which is assumed to drive film flow. Finally, to estimate the film-flow

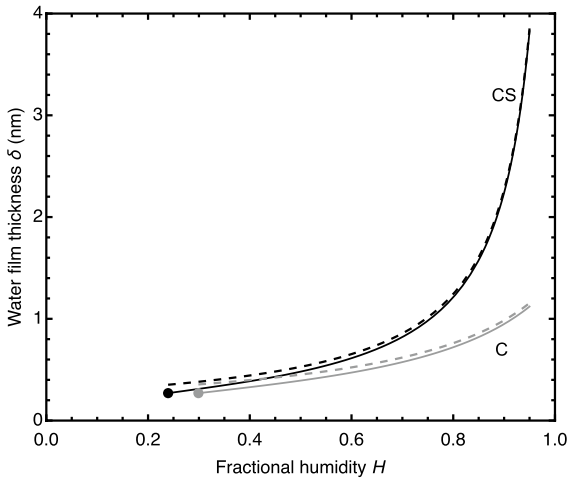

Fig. 13 Variation of water film thickness δ with fractional humidity H for calcium silicate sheet (CS) and dense concrete (C) calculated from GAB isotherms. Solid lines (—) show $\delta(H)$ calculated from Eq. 11, 13 with experimental values m_G 0.00522, k_G 0.979, c_G 10.67 for CS (authors' unpublished data, 25 °C), and m_G 0.0121, k_G 0.802, c_G 9.853 for concrete C ([39], temperature not stated); dashed lines (- -) show $\delta(H)$ calculated from the approximate form of Eq. 11, $F = m_G/(1 - k_G H)$; ● (CS) ● (C) mark values of H_m

contribution to the overall mass flux in the cup test k_{mf} is scaled by the film cross-section area per unit cross-section of the bulk solid, $F_v = \theta = F\rho_b/\rho_w$ and also by a geometrical tortuosity factor G. For dimensional consistency with D_v, the driving force for flow is expressed in terms of the water vapour pressure $p_w = p_{w0}H$ via the relation $dp_c/dx = (\rho_w \mathbf{R}T/M_w p_w) \cdot dp_w/dx$ Then the film flow contribution to D_v, valid for $H > H_m$, is

$$D_{vf} = \frac{G\rho_b\rho_w \mathbf{R}T}{3\eta M_w p_{w0}} \cdot \frac{F\delta^2}{H} = \beta \cdot \frac{F^3}{H}. \quad (13)$$

The quantity $\beta = G\rho_b\rho_w \mathbf{R}T\delta_m^2/(3\eta M_w p_{w0} m_G^2)$, dimension T, does not depend on H. If film flow is to make a discernible contribution to the overall mass flux under wet-cup conditions the quantity D_{vf} must be of a similar magnitude to D_{v0}. For calcium silicate sheet all quantities in Eq. 13 are known with good accuracy, except for G which we take to lie in the range 0.05–0.5. Using the GAB parameter values for calcium silicate sheet given in the caption to Fig. 13 and $\eta = 8.90 \times 10^{-3}$ Pa s, $p_{w0} = 3.17$ kPa, $\rho_b = 270$ kg m^{-3}, and $G = 0.1$ yields values for D_{vf} at 25 °C and $H = 0.7, 0.8$ and 0.9 of 6.7×10^{-12} s, 1.9×10^{-11} s and 1.0×10^{-10} s respectively. These should be compared with the Hellmann value of D_{v0} 1.85×10^{-10} s.

References

1. ASTM (2016) E96:16 Standard test methods for water vapor transmission of materials. ASTM, W Conshohocken, PA
2. British Standards Institution (1999) EN 1015-19:1999 Methods of test for mortar for masonry—Part 19: Determination of water vapour permeability of hardened rendering and plastering mortars. BSI Standards Ltd, London
3. British Standards Institution (2016) EN ISO 12572:2016 Hygrothermal performance of building materials and products—Determination of water vapour transmission properties—Cup method (ISO 12572:2016). BSI Standards Ltd, London
4. British Standards Institution (2009) EN 15803:2009 Conservation of cultural property—Test methods—Determination of water vapour permeability (δ_p). BSI Standards Ltd, London
5. Joy FA, Wilson AG (1963) Standardization of the dish method for measuring water vapor transmission. In: Proceedings of the international symposium on humidity and moisture, Washington DC, vol 4, pp 259–273. (Division of Building Research, National Research Council of Canada, Research paper no 279, 1966)
6. Bomberg M (1989) Testing water vapor transmission: Unresolved issues. In: Trechsel HR, Bomberg M (eds) Water vapor transmission through building materials and systems: Mechanisms and measurement, ASTM STP 1039, pp 157–167. (American Society for Testing and

Materials, Philadelphia PA. (Institute for Research in Construction, National Research Council of Canada, IRC paper no 1615)
7. Galbraith GH, McLean RC, Tao Z, Kang N (1992) The comparability of water vapour permeability measurements. Build Res Inf 20(6):364–372. https://doi.org/10.1080/09613219208727245
8. Roels S, Carmeliet J, Hens H, Adan O, Brocken H, Cerny R, Pavlik Z, Hall C, Kumaran K, Pel L, Plagge R (2004) Interlaboratory comparison of hygric properties of porous building materials. J Therm Envel Build Sci 27(4):307–325. https://doi.org/10.1177/1097196304042119
9. Feng C, Guimarães AS, Ramos N, Sun L, Gawin D, Konca P, Hall C, Zhao J, Hirsch H, Grunewald J et al (2020) Hygric properties of porous building materials (VI): A round robin campaign. Build Environ 185:107242. https://doi.org/10.1016/j.buildenv.2020.107242
10. Hall C, Hoff WD (2021) Water transport in brick, stone and concrete, 3rd edn. CRC Press, Boca Raton
11. Kumaran M (1998) An alternative procedure for the analysis of data from the cup method measurements for determination of water vapor transmission properties. J Test Eval 26:575–581. https://doi.org/10.1520/JTE12115J
12. Hall C, Lo GJ, Hamilton A (2021) Sharp front analysis of moisture buffering. RILEM Tech Lett 6:78–81. https://doi.org/10.21809/rilemtechlett.2021.136
13. Hall C, Lo GJ, Hamilton A (2022) Measuring water vapour permeability using remote-reading humidity sensors. Meas Sci Technol 34(2):027004. https://doi.org/10.1088/1361-6501/ac9f5f
14. Schirmer R (1938) Die Diffusionzahl von Wasserdampf-Luft-Gemischen und die Verdampfungsgeschwindigkeit. Z des VDI Beih Verfahr 6:170–177
15. Massman W (1998) A review of the molecular diffusivities of H_2O, CO_2, CH_4, CO, O_3, SO_2, NH_3, N_2O, NO, and NO_2 in air, O_2 and N_2 near STP. Atmos Environ 32(6):1111–1127. https://doi.org/10.1016/S1352-2310(97)00391-9
16. Hellmann R (2020) Reference values for the cross second virial coefficients and dilute gas binary diffusion coefficients of the systems (H_2O + air) and (H_2O + air) from first principles. J Chem Eng Data 65(8):4130–4141. https://doi.org/10.1021/acs.jced.0c00465
17. Vololonirina O, Perrin B (2016) Inquiries into the measurement of vapour permeability of permeable materials. Constr Build Mater 102:338–348. https://doi.org/10.1016/j.conbuildmat.2015.10.126
18. Feng C, Janssen H (2021) Hygric properties of porous building materials (VII): Full-range benchmark characterizations of three materials. Build Environ 195:107727. https://doi.org/10.1016/j.buildenv.2021.107727
19. Fabbri A, Morel JC, Aubert J-E, Bui Q-B, Gallipoli D, Ventura A, Reddy VB, Hamard E, Pele-Peltier A, Abhilash HN (2021) An overview of the remaining challenges of the RILEM TC 274-TCE, testing and characterisation of earth-based building materials and elements. RILEM Techn Lett 6:150–157
20. Greenspan L (1977) Humidity fixed points of binary saturated aqueous solutions. J Res Natl Bureau Stand Sect A Phys Chem 81(1):89–96. https://doi.org/10.6028/jres.081A.011
21. ASTM (2020) E104:20a Standard practice for maintaining constant relative humidity by means of aqueous solutions. ASTM, W Conshohocken, PA
22. Pollio M, Kitic D, Favetto G, Chirife J (1988) A note about the correct water activity value of saturated potassium nitrate at 25° C. Lebensm Wiss Technol 21(1):66–67
23. Pollio M, Kitic D, Resnik S (1996) Research Note: A_w values of six saturated salt solutions at 25° C. Re-examination for the purpose of maintaining a constant relative humidity in water sorption measurements. Lebensm Wiss Technol 29(4):376–378. https://doi.org/10.1006/fstl.1996.0058
24. Apelblat A, Korin E (1998) Vapour pressures of saturated aqueous solutions of ammonium iodide, potassium iodide, potassium nitrate, strontium chloride, lithium sulphate, sodium thiosulphate, magnesium nitrate, and uranyl nitrate from T = (278 to 323) K. J Chem Thermodyn 30(4):459–471. https://doi.org/10.1006/jcht.1997.0311
25. Zeng D, Wu Z, Yao Y, Han H (2010) Isopiestic determination of water activity on the system $LiNO_3$ + KNO_3 + H_2O at 273.1 and 298.1 K. J Solut Chem 39:1360–1376. https://doi.org/10.1007/s10953-010-9582-1
26. Lach A, André L, Guignot S, Christov C, Henocq P, Lassin A (2018) A Pitzer parametrization to predict solution properties and salt solubility in the H − Na − K − Ca − Mg − NO_3 − H_2O system at 298.15 K. J Chem Eng Data 63(3):787–800. https://doi.org/10.1021/acs.jced.7b00953
27. Tereshchenko AG (2020) Dynamic method for the determination of hygroscopicity of water-soluble solids. J Solut Chem 49(7–8):1029–1051. https://doi.org/10.1007/s10953-020-01007-w
28. Monnin C, Dubois M, Papaiconomou N, Simonin J-P (2002) Thermodynamics of the LiCl + H_2O system. J Chem Eng Data 47(6):1331–1336. https://doi.org/10.1021/je0200618
29. Zeng D, Zhou J (2006) Thermodynamic consistency of the solubility and vapor pressure of a binary saturated salt + water system. 1. LiCl + H_2O. J Chem Eng Data 51(2):315–321. https://doi.org/10.1021/je050322o
30. Apelblat A (1993) The vapour pressures of saturated aqueous lithium chloride, sodium bromide, sodium nitrate, ammonium nitrate, and ammonium chloride at temperatures from 283 K to 313 K. J Chem Thermodyn 25(1):63–71. https://doi.org/10.1006/jcht.1993.1008
31. Van Den Bulck E (1990) Isotherm correlation for water vapor on regular-density silica gel. Chem Eng Sci 45(5):1425–1429. https://doi.org/10.1016/0009-2509(90)87138-I
32. Wang Y, LeVan MD (2009) Adsorption equilibrium of carbon dioxide and water vapor on zeolites 5A and 13X and silica gel: Pure components. J Chem Eng Data 54(10):2839–2844. https://doi.org/10.1021/je800900a
33. Pitzer KS, Oakes CS (1994) Thermodynamics of calcium chloride in concentrated aqueous solutions and in

crystals. J Chem Eng Data 39(3):553–559. https://doi.org/10.1021/je00015a035
34. Zeng D, Xu W, Voigt W, Yin X (2008) Thermodynamic study of the system (LiCl + $CaCl_2$ + H_2O). J Chem Thermodyn 40(7):1157–1165. https://doi.org/10.1016/j.jct.2008.02.010
35. British Standards Institution: EN 12086:2013 Thermal insulating products for building applications—Determination of water vapour transmission properties. BSI Standards Ltd, London (2013)
36. Besley L, Bottomley G (1969) The water vapour equilibria over magnesium perchlorate hydrates. J Chem Thermodyn 1(1):13–19
37. Robertson K, Bish D (2011) Stability of phases in the $Mg(ClO_4)_2 \cdot nH_2O$ system and implications for perchlorate occurrences on Mars. J Geophys Res Planets. https://doi.org/10.1029/2010JE003754
38. Ranesi A, Veiga MR, Faria P (2021) Laboratory characterization of relative humidity dependent properties for plasters: A systematic review. Constr Build Mater 304:124595. https://doi.org/10.1016/j.conbuildmat.2021.124595
39. Kumaran M (1996) Heat, air and moisture transfer through new and retrofitted insulated envelope parts, Final report, IEA-Annex 24, Task 3: Material Properties. IRC/NRC
40. International Energy Agency (1991) Condensation and energy, IEA Annex XIV, vol 3, Catalogue of Material Properties, IEA
41. Carmeliet J, Roels S (2001) Determination of the isothermal moisture transport properties of porous building materials. J Therm Envel Build Sci 24(3):183–210. https://doi.org/10.1106/Y6T2-9LLP-04Y5-AN6T
42. Pavlík Z, Žumár J, Pavlíková M, Kočí J, Černý R (2012) Investigation of water vapour transport properties of gypsum using genetic algorithm. Int J Civ Environ Eng 6(10):821–826. https://doi.org/10.5281/zenodo.1071282
43. Vereecken E, Van De Walle W, Roels S (2019) A novel and flexible test setup to measure the vapour diffusion resistance of building materials and wall components. MATEC Web Conf. https://doi.org/10.1051/matecconf/201928202057
44. Zhang Y, Zheng Y, Huang J (2022) Determination of water vapor transmission properties of sandstones in the Yungang Grottoes. Int J Archit Herit 1--13. https://doi.org/10.1080/15583058.2022.2147878
45. Ruedrich J, Bartelsen T, Dohrmann R, Siegesmund S (2011) Moisture expansion as a deterioration factor for sandstone used in buildings. Environ Earth Sci 63:1545–1564. https://doi.org/10.1007/s12665-010-0767-0
46. Stück H, Siegesmund S, Rüdrich J (2011) Weathering behaviour and construction suitability of dimension stones from the Drei Gleichen area (Thuringia, Germany). Environ Earth Sci 63:1763–1786. https://doi.org/10.1007/s12665-011-1043-7
47. Banfill P (2021) Hygrothermal simulation of building performance: data for Scottish masonry materials. Mater Struct 54(4):167. https://doi.org/10.1617/s11527-021-01759-x
48. Andrejkovičová S, Maljaee H, Rocha D, Rocha F, Soares MR, Velosa A (2022) Mortars for conservation of late 19th and early 20th century buildings—combination of natural cements with air lime. Materials 15(10):3704. https://doi.org/10.3390/ma15103704
49. Jaroš P, Vertal' M, Slávik R (2023) Hygric and thermal properties of Slovak building sandstones. J Build Eng. https://doi.org/10.1016/j.jobe.2023.105891
50. Dondi M, Principi P, Raimondo M, Zanarini G (2003) Water vapour permeability of clay bricks. Constr Build Mater 17(4):253–258. https://doi.org/10.1016/S0950-0618(02)00117-4
51. Togkalidou T, Karoglou M, Bakolas A, Giakoumaki A, Moropoulou A (2013) Correlation of water vapor permeability with microstructure characteristics of building materials using robust chemometrics. Transp Porous Media 99:273–295. https://doi.org/10.1007/s11242-013-0184-4
52. Galbraith GH, Tao Z, McLean RC (1993) Separation of moisture flow through porous building materials into vapour and liquid components. Build Serv Eng Res Technol 14(3):107–113. https://doi.org/10.1177/014362449301400304
53. Hens H (2009) Vapor permeability measurements: impact of cup sealing, edge correction, flow direction and mean relative humidity. J ASTM Int 6:101893
54. Stück H, Plagge R, Siegesmund S (2013) Numerical modeling of moisture transport in sandstone: the influence of pore space, fabric and clay content. Environ Earth Sci 69:1161–1187. https://doi.org/10.1007/s12665-013-2405-0
55. Alderete N, Zaccardi YV, Di Maio AA, De Belie N (2018) Isothermal water vapour permeability of concrete with different supplementary cementitious materials. Mater Constr 68(330):152–152. https://doi.org/10.3989/mc.2018.v68.i330
56. Hall C, Hamilton A (2015) Porosity-density relations in stone and brick materials. Mater Struct 48:1265–1271. https://doi.org/10.1617/s11527-013-0231-1
57. Hall C, Hamilton A (2016) Porosities of building limestones: using the solid density to assess data quality. Mater Struct 49(10):3969–3979. https://doi.org/10.1617/s11527-015-0767-3
58. Penman H (1940) Gas and vapour movements in the soil: I. The diffusion of vapours through porous solids. J Agric Sci 30(3):437–462. https://doi.org/10.1017/S0021859600048164
59. Philip J, De Vries D (1957) Moisture movement in porous materials under temperature gradients. EOS Trans Am Geophys Union 38(2):222–232. https://doi.org/10.1029/TR038i002p00222
60. Marshall T (1959) The diffusion of gases through porous media. J Soil Sci 10(1):79–82. https://doi.org/10.1111/j.1365-2389.1959.tb00667.x
61. Millington R (1959) Gas diffusion in porous media. Science 130(3367):100–102. https://doi.org/10.1126/science.130.3367.100.b
62. Evans R III, Watson G, Mason E (1961) Gaseous diffusion in porous media at uniform pressure. J Chem Phys 35(6):2076–2083. https://doi.org/10.1063/1.1732211

63. Bear J (1972) Dynamics of fluids in porous media. American Elsevier, New York
64. Suman R, Ruth D (1993) Formation factor and tortuosity of homogeneous porous media. Transp Porous Media 12:185–206. https://doi.org/10.1007/BF00616979
65. Ghanbarian B, Hunt AG (2014) Universal scaling of gas diffusion in porous media. Water Resour Res 50(3):2242–2256. https://doi.org/10.1002/2013WR014790
66. Ray N, Rupp A, Schulz R, Knabner P (2018) Old and new approaches predicting the diffusion in porous media. Transp Porous Media 124:803–824. https://doi.org/10.1007/s11242-018-1099-x
67. Ho CK, Webb SW (2006) Gas transport in porous media, vol 20. Springer, Dordrecht
68. Zhang Z, Thiery M, Baroghel-Bouny V (2016) Investigation of moisture transport properties of cementitious materials. Cem Concr Res 89:257–268. https://doi.org/10.1016/j.cemconres.2016.08.013
69. Tuller M, Or D (2001) Hydraulic conductivity of variably saturated porous media: film and corner flow in angular pore space. Water Resour Res 37(5):1257–1276. https://doi.org/10.1029/2000WR900328
70. McLean RC, Galbraith GH, Sanders G (1990) Moisture transmission testing of building materials and the presentation of vapour permeability values. Build Res Pract J CIB 2:82–91
71. Tokunaga TK (2009) Hydraulic properties of adsorbed water films in unsaturated porous media. Water Resour Res 45(6):W06415. https://doi.org/10.1029/2009WR007734
72. Lebeau M, Konrad J-M (2010) A new capillary and thin film flow model for predicting the hydraulic conductivity of unsaturated porous media. Water Resour Res 46(12):W12554. https://doi.org/10.1029/2010WR009092
73. Peters A (2013) Simple consistent models for water retention and hydraulic conductivity in the complete moisture range. Water Resour Res 49(10):6765–6780. https://doi.org/10.1002/wrcr.20548
74. Zhao J, Feng S, Grunewald J, Meissner F, Wang J (2022) Drying characteristics of two capillary porous building materials: calcium silicate and ceramic brick. Build Environ 216:109006. https://doi.org/10.1016/j.buildenv.2022.109006
75. Pietrak K, Kubiś M, Furmański P, Seredyński M, Wasik M, Wiśniewski T, Łapka P (2019) Measurement of thermal, hygric and physical properties of bricks and mortar common for the polish market. In: IOP conference series: Materials science and engineering, vol 660, 012022. https://doi.org/10.1088/1757-899X/660/1/012022
76. Koronthalyova O, Bagel L, Kuliffayova M, Ifka T (2015) Effect of presence of salt on hygric performance of ceramic bricks. Transp Porous Media 107:667–682. https://doi.org/10.1007/s11242-015-0461-5
77. Graue B, Siegesmund S, Middendorf B (2011) Quality assessment of replacement stones for the Cologne Cathedral: mineralogical and petrophysical requirements. Environ Earth Sci 63:1799–1822. https://doi.org/10.1007/s12665-011-1077-x
78. Keppert M, Žumár J, Čáchová M, Koňáková D, Svora P, Pavlík Z, Vejmelkova E, Černý R (2016) Water vapor diffusion and adsorption of sandstones: influence of rock texture and composition. Adv Mater Sci Eng. https://doi.org/10.1155/2016/8039748
79. Kočí V, Maděra J, Fořt J, Žumár J, Pavlíková M, Pavlík Z, Černý R (2014) Service life assessment of historical building envelopes constructed using different types of sandstone: a computational analysis based on experimental input data. Sci World J. https://doi.org/10.1155/2014/802509
80. Pavlík Z, Michálek P, Pavlíková M, Kopecká I, Maxová I, Černý R (2008) Water and salt transport and storage properties of Mšené sandstone. Constr Build Mater 22(8):1736–1748. https://doi.org/10.1016/j.conbuildmat.2007.05.010
81. Stempf A, Muller P, Pabon M, Corpart J (1999) Fluorinated acrylics as an alternative for hydrophobic and oleophobic coating for stone and concrete. Int J Restor Build Monum 5:273–288
82. Roberts JN, Schwartz LM (1985) Grain consolidation and electrical conductivity in porous media. Phys Rev B 31(9):5990. https://doi.org/10.1103/PhysRevB.31.5990
83. Miller AZ, Dionísio A, Laiz L, Macedo MF, Saiz-Jimenez C (2009) The influence of inherent properties of building limestones on their bioreceptivity to phototrophic microorganisms. Ann Microbiol 59(4):705–713. https://doi.org/10.1007/BF03179212
84. Pia G (2016) Fluid flow in complex porous media: experimental data and IFU model predictions for water vapour permeability. J Nat Gas Sci Eng 35:283–290. https://doi.org/10.1016/j.jngse.2016.08.053
85. Cabrera V, Lopez-Vizcaino R, Yustres A, Ruiz MÁ, Torrero E, Navarro V (2020) A functional structure for state functions of moisture transfer in heritage building elements. J Build Eng 29:101201. https://doi.org/10.1016/j.jobe.2020.101201
86. Cascione V, Maskell D, Shea A, Walker P, Mani M (2020) Comparison of moisture buffering properties of plasters in full scale simulations and laboratory testing. Constr Build Mater 252:119033. https://doi.org/10.1016/j.conbuildmat.2020.119033
87. Koňáková D, Čáchová M, Vejmelkova E, Keppert M, Jerman M, Bayer P, Rovnaníková P, Černý R (2017) Lime-based plasters with combined expanded clay-silica aggregate: microstructure, texture and engineering properties. Cement Concr Compos 83:374–383. https://doi.org/10.1016/j.cemconcomp.2017.08.005
88. Čáchová M, Vejmelkova E, Koňáková D, Žumár J, Keppert M, Reiterman P, Černý R (2016) Application of ceramic powder as supplementary cementitious material in lime plasters. Mater Sci 22(3):440–444. https://doi.org/10.5755/j01.ms.22.3.7433
89. Fusade L, Viles H, Wood C, Burns C (2019) The effect of wood ash on the properties and durability of lime mortar for repointing damp historic buildings. Constr Build Mater 212:500–513. https://doi.org/10.1016/j.conbuildmat.2019.03.326
90. Aly M, Pavia S (2019) Limestone-filled, hydraulic-lime mortars for historic and traditional fabrics. In: 5th Historic mortars conference (HMC 2019), Pamplona
91. Zemanova L, Pokorny J, Pavlikova M, Pavlik Z (2019) Hygric properties of cement-lime plasters with

incorporated lightweight mineral admixture. In: IOP conference series: Materials science and engineering, vol 603, 022046. https://doi.org/10.1088/1757-899X/603/2/022046
92. Posani M, Veiga R, de Freitas VP (2022) Thermal mortar-based insulation solutions for historic walls: an extensive hygrothermal characterization of materials and systems. Constr Build Mater 315:125640. https://doi.org/10.1016/j.conbuildmat.2021.125640
93. Záleská M, Pavlíková M, Pivák A, Lauermannová A-M, Jankovskỳ O, Pavlík Z (2021) Lightweight vapor-permeable plasters for building repair: detailed experimental analysis of the functional properties. Materials 14(10):2613. https://doi.org/10.3390/ma14102613
94. Jerman M, Keppert M, Vỳbornỳ J, Černý R (2013) Hygric, thermal and durability properties of autoclaved aerated concrete. Constr Build Mater 41:352–359. https://doi.org/10.1016/j.conbuildmat.2012.12.036
95. Giosuè C, Pierpaoli M, Mobili A, Ruello ML, Tittarelli F (2017) Influence of binders and lightweight aggregates on the properties of cementitious mortars: from traditional requirements to indoor air quality improvement. Materials 10(8):978. https://doi.org/10.3390/ma10080978
96. Fouchal F, Gouny F, Maillard P, Ulmet L, Rossignol S (2015) Experimental evaluation of hydric performances of masonry walls made of earth bricks, geopolymer and wooden frame. Build Environ 87:234–243. https://doi.org/10.1016/j.buildenv.2015.01.036
97. Cagnon H, Aubert J-E, Coutand M, Magniont C (2014) Hygrothermal properties of earth bricks. Energy Build 80:208–217. https://doi.org/10.1016/j.enbuild.2014.05.024
98. Maillard P, Aubert J-E (2014) Effects of the anisotropy of extruded earth bricks on their hygrothermal properties. Constr Build Mater 63:56–61. https://doi.org/10.1016/j.conbuildmat.2014.04.001
99. Liuzzi S, Hall M, Stefanizzi P, Casey S (2013) Hygrothermal behaviour and relative humidity buffering of unfired and hydrated lime-stabilised clay composites in a Mediterranean climate. Build Environ 61:82–92. https://doi.org/10.1016/j.buildenv.2012.12.006
100. Hansen EJdP, Hansen KK (2002) Unfired clay bricks—moisture properties and compressive strength. In: 6th Symposium on building physics in Nordic countries, pp 453–460
101. McGregor F, Heath A, Fodde E, Shea A (2014) Conditions affecting the moisture buffering measurement performed on compressed earth blocks. Build Environ 75:11–18
102. Maskell D, Thomson A, Walker P, Lemke M (2018) Determination of optimal plaster thickness for moisture buffering of indoor air. Build Environ 130:143–150. https://doi.org/10.1016/j.buildenv.2017.11.045
103. Hamilton A, Hall C (2005) Physicochemical characterization of a hydrated calcium silicate board material. J Build Phys 29(1):9–19. https://doi.org/10.1177/1744259105053280
104. Hamilton A, Hall C (2007) A note on the density of a calcium silicate hydrate board material. J Build Phys 31(1):69–71. https://doi.org/10.1177/1744259107080818
105. Tuominen O, Tuominen E, Vainio M, Ruuska T, Vinha J (2019) Thermal and moisture properties of calcium silicate insulation boards. In: MATEC web of conferences vol 282, p 02065. https://doi.org/10.1051/matecconf/201928202065
106. Fořt J, Pavlík Z, Žumár J, Pavlíková M, Černý R (2014) Effect of temperature on water vapor transport properties. J Build Phys 38(2):156–169. https://doi.org/10.1177/1744259114532612
107. Richter J, Staněk K (2016) Measurements of water vapour permeability-tightness of fibreglass cups and different sealants and comparison of μ-value of gypsum plaster boards. Procedia Eng 151:277–283. https://doi.org/10.1016/j.proeng.2016.07.377
108. Padfield T (1998) The role of absorbent building materials in moderating changes of relative humidity. PhD thesis, Department of Structural Engineering and Materials, Technical University of Denmark
109. Padfield T (1999) Humidity buffering of the indoor climate by absorbent walls. In: Proceedings of the 5th symposium on building physics in the Nordic countries. Chalmers University of Technology, Göteborg, vol 2, pp 637–644
110. Mukhopadhyaya P, Kumaran MK, Lackey J (2005) Use of the modified cup method to determine temperature dependency of water vapor transmission properties of building materials. J Test Eval 33(5):316
111. Knarud JI, Kvande T, Geving S (2022) Modelling hydraulic conductivity for porous building materials based on a prediction of capillary conductivity at capillary saturation. Int J Heat Mass Transf 186:122457. https://doi.org/10.1016/j.ijheatmasstransfer.2021.122457
112. Scheffler GA, Plagge R (2010) A whole range hygric material model: Modelling liquid and vapour transport properties in porous media. Int J Heat Mass Transf 53(1–3):286–296. https://doi.org/10.1016/j.ijheatmasstransfer.2009.09.030
113. Galbraith GH, McLean RC, Tao Z (1993) Vapour permeability: suitability and consistency of current test procedures. Build Serv Eng Res Technol 14(2):67–70. https://doi.org/10.1177/014362449301400205
114. ISO 4793:1980 Laboratory sintered (fritted) filters: porosity grading, classification and designation. International Organization for Standardization, Geneva (1980)
115. Webster CE, Drago RS, Zerner MC (1998) Molecular dimensions for adsorptives. J Am Chem Soc 120(22):5509–5516. https://doi.org/10.1021/ja973906m
116. Bird RB, Stewart WE, Lightfoot EN (1960) Transport phenomena. Wiley, New York